Nano Energy 63 (2019) 103886

Contents lists available at ScienceDirect

Nano Energy

journal homepage: www.elsevier.com/locate/nanoen

Communication

Plasmon-enhanced photo(electro)chemical nitrogen fixation under ambient conditions using visible light responsive hybrid hollow Au-Ag_2O nanocages

Mohammadreza Nazemi[a,b], Mostafa A. El-Sayed[a,*]

[a] Laser Dynamics Laboratory, School of Chemistry and Biochemistry, Georgia Institute of Technology, Atlanta, GA, 30332-0400, USA
[b] George W. Woodruff School of Mechanical Engineering, Georgia Institute of Technology, Atlanta, GA, 30332-0405, USA

ARTICLE INFO

Keywords:
Plasmonic photocatalysis
Nitrogen fixation
Visible-light responsive
Hybrid plasmonic-semiconductor

ABSTRACT

Photo(electro)catalytic N_2 fixation with water under ambient conditions offers an ideal pathway for clean, sustainable, and decentralized ammonia production and might serve as a potential alternative to the capital and energy intensive Haber-Bosch process. To date, almost all photocatalysts for nitrogen reduction reaction (NRR) suffer from poor selectivity, low activity due to the difficulty in breaking the strong N≡N bond, competition with the more favorable hydrogen evolution reaction (HER), and inefficient utilization of the solar spectrum. Here, a photo(electro)chemical setup is demonstrated using a hybrid plasmonic-semiconductor as an active photocatalyst under visible light. Hybrid hollow Au–Ag_2O nanocages are utilized to convert atmospheric N_2 to NH_3 in a pure water system without using sacrificial reagents. The average NH_3 production rate of 28.2 mg m^{-2} h^{-1} and the solar-to-ammonia (STA) conversion efficiency of 0.017% are achieved under one sun illumination. The apparent quantum efficiency of 1.2% for NH_3 production is obtained with the monochromatic light source at 685 nm, which is among the highest ever-reported values for the photocatalytic NRR. The isotopic labeling experiments using $^{15}N_2$ confirms that supplied N_2 gas is the only source of NH_3 formation in the system. This work showcases the application of plasmonic photocatalysis in the challenging multi-electron nitrogen fixation.

1. Introduction

Ammonia is one of the widely produced chemicals in the world, with broad applications in producing agricultural fertilizer, energy, and in the pharmaceutical industry [1–5]. Photocatalytic nitrogen fixation for "green ammonia" synthesis, using water as a reducing reagent and sunlight under ambient conditions, provides an attractive route for clean, sustainable, and distributed ammonia synthesis. This approach might serve as an alternative to the Haber-Bosch process, particularly in remote areas where access to the centralized infrastructure or pipelines is limited [6].

To date, almost all photocatalysts for nitrogen reduction reaction (NRR) suffer from poor selectivity, low activity due to the difficulty in breaking the strong N≡N bond, competition with the more favorable hydrogen evolution reaction (HER), and inefficient utilization of the solar spectrum. Superior light absorption, efficient photo-excited charge separation, and transfer, and the ability to drive photocatalytic redox reactions are the key elements to the rational design of an efficient photocatalyst for the nitrogen reduction reaction (NRR) [7]. The photocatalytic redox system using water as a reducing reagent comprises water oxidation at the valence band through the reaction of water with photo-generated holes (h^+) (Equation (1)) and NRR at the conduction band through the reaction of N_2, protons (H^+), and photo-generated electrons (Equation (2)) [8]:

$$3H_2O + 6h^+ \rightarrow \frac{3}{2}O_2 + 6H^+ \quad (1)$$

$$N_2 + 6H^+ + 6e^- \rightarrow 2NH_3 \quad (2)$$

The overall reaction, with the Gibbs free energy (ΔG^o) of 339 kJ mol^{-1} for ammonia formation from water and N_2, is:

$$N_2 + 3H_2O \rightarrow 2NH_3 + \frac{3}{2}O_2 \quad (3)$$

To date, most studies on photocatalytic nitrogen fixation have focused on wide bandgap semiconductors (usually metal oxides) such as TiO_2 (E_g = 3.2 eV) owing to its abundance, and its high and stable light absorption capability in the UV region. TiO_2 has exhibited moderate NRR activity when incorporated with transition metal dopants (e.g., Fe, Mo, Ru) or through introducing oxygen vacancies at the surface of the photocatalyst [8–13]. Wide bandgap semiconductors show weak absorption under visible and IR light and therefore, low NRR activity when the wavelength of the incident light is higher than 400 nm. It is

* Corresponding author.
E-mail address: melsayed@gatech.edu (M.A. El-Sayed).

https://doi.org/10.1016/j.nanoen.2019.103886
Received 18 May 2019; Received in revised form 6 July 2019; Accepted 6 July 2019
Available online 08 July 2019

important to note that only 5% of the solar irradiation spectrum received on earth's surface is UV ($\lambda < 400$ nm), while 50% is in the visible region (400 nm < λ < 800 nm) and the remaining 45% is in the IR region ($\lambda > 800$ nm). Therefore, the development of a photocatalyst that is active in the incident photon wavelength of greater than 400 nm is necessary to harvest most of the solar irradiation spectrum and enhance the solar-to-ammonia (STA) efficiency (η_{STA}). Recently, it was demonstrated that using oxygen vacancy rich BiOBr nanosheets can enhance the photocatalytic NRR activity under visible light in water, yet there is room to improve the apparent quantum efficiency (η_{AQE}) [14–16].

Under the stimulus of light, some noble metal nanoparticles, such as Au and Ag, undergo a process called localized surface plasmon resonance (LSPR), which is the collective oscillation of free electrons at the material's surface [7]. The strong electromagnetic plasmon fields generated under light illumination can be utilized for various applications in photocatalysis and sensing [17–23]. The placement of plasmonic nanostructures in close proximity (< 10 nm) to each other results in an enhanced electromagnetic field in the interparticle gap [24].

In our previous studies, we showed that hollow Au nanocages (AuHNCs) are an active electrocatalyst for the conversion of N_2 to NH_3 in an ionic aqueous solution under ambient conditions, with Faradaic efficiency exceeding 35% owing to the "cage effect" (confinement of reactants in the cavity), high active surface area, and high electrocatalytic NRR activity on Au surfaces [25,26]. Here, hybrid Au–Ag_2O nanocages are synthesized through a facile oxidation process, allowing for the coupling of the plasmonic enhancement of Au nanocages with visible-light active p-type Ag_2O to achieve superior photocatalytic NRR performance under ambient conditions using water as an electron donor and sunlight. While several studies on photocatalytic NRR using hybrid plasmonic-semiconductor photocatalysts have been performed [27–30], very few have coupled a plasmonic metal and semiconductor that are both active under visible light [22]. Combining the two increases the photo-generated electrons' concentration upon visible light illumination for photocatalytic NRR. As the work function of the p-type semiconductor (Ag_2O) is higher than that of the Au plasmonic metal ($\varnothing_S > \varnothing_M$), a Schottky barrier is formed where the photo-generated holes of Ag_2O are transferred to the Au plasmonic metal at the metal-semiconductor interface so that the Fermi levels in the metal and semiconductor are aligned [31,32]. Energy bands in Ag_2O bend downward to match the chemical potentials. Photo-generated electron transfer from the conduction band of Ag_2O to the surface of the Au nanoparticles occurs, and/or so-called "hot-electrons" are injected from the Au nanoparticle surface to the conduction band of Ag_2O. Both electron transfer processes are possible and competitive. It has been demonstrated that transition metal loaded titania results in smaller ammonia yield than bare titania if Ti^{3+} active sites on the surface are blocked by transition metals, giving experimental proof of these competing phenomenon [10]. In our nanocages, Au and Ag_2O nanoparticles are settled adjacent to each other whereby both can act as an active site in the interior or at the exterior surface of the nanocages for nitrogen adsorption and reduction, enabling us to achieve superior selectivity and efficiency for the NRR.

2. Results and discussion

Bimetallic porous Au–Ag nanocages with various LSPR peak positions and pore sizes are prepared by adding $HAuCl_4$ (aq.) solution to the solid silver nanocubes (AgNCs) solution through the galvanic replacement method [20]. By oxygenating the Au–Ag nanocages through purging the solution with pure oxygen gas, Ag is oxidized to silver (I) oxide (Ag_2O) at room temperature, an extremely stable metal oxide semiconductor in ambient conditions [33]. After oxygen treatment of the Au–Ag nanocages, the LSPR peak position slightly redshifts (e.g., 15 nm for Au–Ag-670), suggesting the formation of Ag_2O in the cavity and successful synthesis of Ag_2O–Au nanocages (Fig. S1). Ag_2O–Au nanocages with various LSPR peak positions (i.e., 655, 685, and 715 nm) are prepared by increasing the amount of Au^{3+} ions added to the AgNCs template (Fig. 1A). As Ag atoms are etched and replaced by Au atoms, the LSPR peak position redshifts and the pore size at the walls and corners of the nanocages increases (Fig. 1B, C, D). The detailed information regarding the LSPR peak values before and after oxygen treatment of bimetallic Au–Ag nanocages, and the nanocages' Au and Ag content is provided in the supporting information (Table S1). High-resolution transmission electron microscopy (HRTEM) and the Fast Fourier Transform (FFT) of 100 oriented Ag_2O–Au nanocages reveals that Ag_2O has the same orientation as Au (Fig. 1E). Furthermore, the measurement of lattice spacings of Ag_2O (Ag–O atomic spacing, 2.23Å) and Au (Au–Au atomic spacing, 2.68Å) in the Ag_2O–Au-685 nanoparticles obtained from HRTEM confirms the formation of Ag_2O after oxygen treatment; these measurements are also comparable with previously reported data obtained by extended x-ray absorption fine structure (EXAFS), (Fig. 1F) [34,35].

X-ray photoelectron spectroscopy (XPS) measurements are performed to investigate the surface elemental composition and the chemical states of the as-prepared Ag_2O, Ag–Au, and Ag_2O–Au nanoparticles. The XPS survey spectra reveal that Ag_2O–Au and Ag–Au nanocages contain Ag 3d, Au 4f, and O 1s, while Ag 3d and O 1s are observed for Ag_2O (Fig. 2A). A pair of spin-orbit doublets with energy peaks at 84.0 eV and 87.7 eV correspond to Au $4f_{7/2}$ and Au $4f_{5/2}$, indicating the existence of Au^o (Au–Au bonding) in Ag_2O–Au and Ag–Au nanocages, while as expected no Au bonding energy peaks are observed for Ag_2O from the high-resolution XPS spectra of Au 4f (Fig. 2B) [36]. The doublet peaks at 368.0 eV and 374.0 eV are assigned to the Ag $3d_{5/2}$ and Ag $3d_{3/2}$, for Ag_2O–Au and Ag_2O, while a slight shift to high binding energy (0.1 eV) is observed for Ag–Au, which distinguishes between Ag^o (Ag–Ag bonding) and Ag^+ (Ag–O bonding) (Fig. 2C) [37]. The O 1s profiles for Ag_2O and Ag_2O–Au are deconvoluted into two peaks centered at 531.5 eV and 532.6 eV (with 0.1 eV negative shift to lower binding energy for Ag_2O–Au), which are attributed to the lattice oxygen atoms of Ag_2O and the chemisorbed oxygen caused by the external ^-OH group or the water molecule adsorbed on the surface (Fig. 2D) [37,38]. The latter peak is also observed in the O 1s profile for Ag–Au nanocages. The same O 1s profiles trend as that for Ag–Au-670 and Ag_2O–Au-685 is observed for O 1s profiles of Ag–Au-645, Ag_2O–Au-655, Ag–Au-710, and Ag_2O–Au-715 (Fig. S2).

The electronic band structures of Ag_2O and Ag_2O–Au-685 nanocages are determined by optical band gaps and ultraviolet photoelectron spectroscopy (UPS) results (Fig. 3A). The summation of the valence band offset at low binding energy (E_F-E_{VBM}) and the secondary electron onset, referenced to the 21.21 eV helium source energy (work function, E_{VAC}-E_F), provides the position of the valence band maximum (E_{VBM}) (Fig. S3). The Fermi level of Au has been reported to be 5.1 eV [21]. The optical band gap is calculated by measuring UV–Vis spectra of the photocatalysts. The UV–Vis spectra are analyzed by the Kubelka–Munk (KM) theory, where an inflection tangent is drawn in the linear portion of the KM function versus the energy of light absorbed (Fig. S4) [39–41]. The band gap energies (E_g) of Ag_2O and Ag_2O–Au are calculated to be 2.34 and 1.6 eV, suggesting that both photocatalysts are visible-light responsive. It is important to note that the modified band gap of 1.6 eV corresponds to the hybrid Ag_2O–Au after structural and chemical modifications of AgNCs and Ag–Au nanocages. The E_{VBM} levels of Ag_2O (1.57 V) and Ag_2O–Au (1.47 V) are more positive than 1.23 V vs. RHE, indicating that both photocatalysts can drive water oxidation (Equation (1)) through photo-generated holes, a necessary reaction to provide protons for NRR (Equation (2)). In addition, the energy levels of the conduction band minimum (E_{CBM}) for Ag_2O (−0.77 V) and Ag_2O–Au (−0.13 V) are more negative than the NRR potential (0.05 V vs. RHE), suggesting that direct photocatalytic nitrogen reduction is possible on the surface of photocatalysts without the need for the sacrificial reagent. The E_{VBM} of photocatalysts is not favorable for the nitrogen oxidation reaction (N_2/NO), as nitrogen's

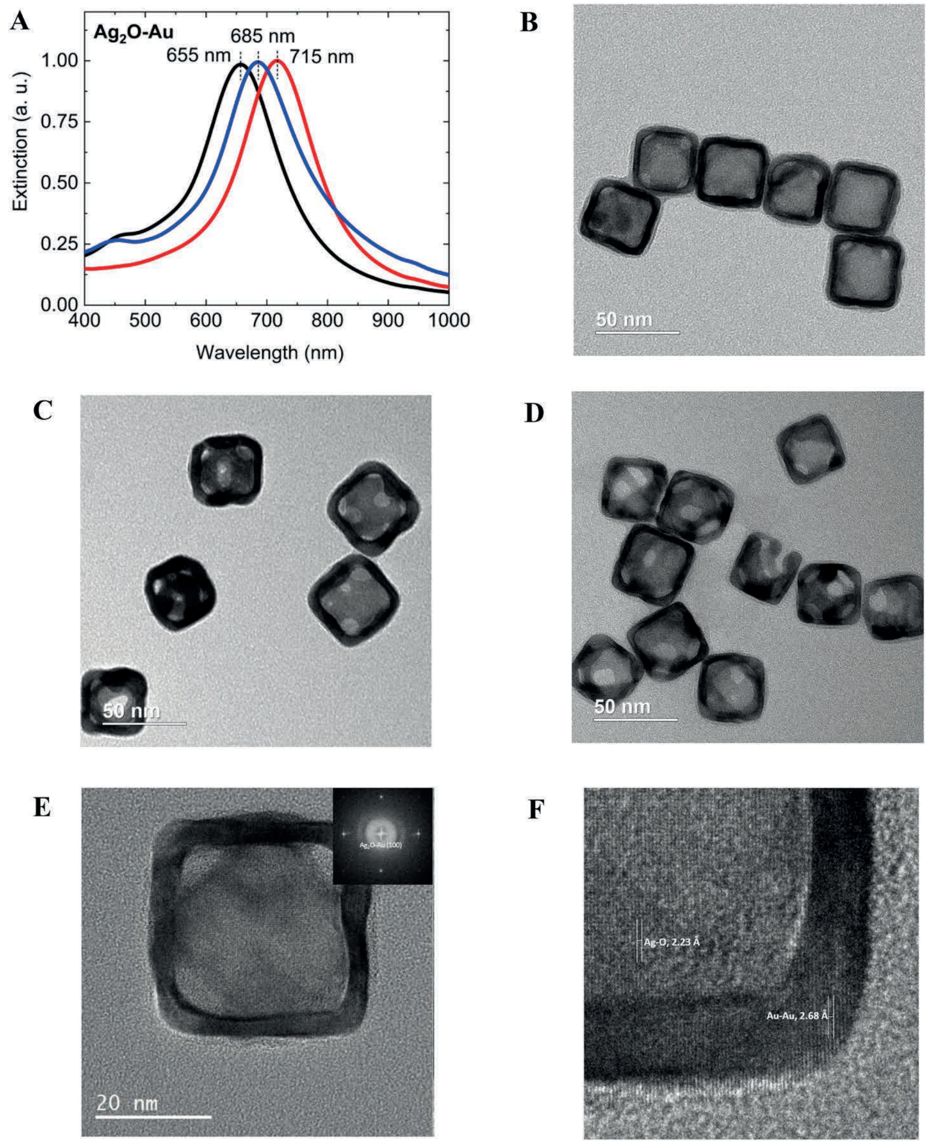

Fig. 1. A) UV–Vis extinction spectra of Ag_2O–Au nanocages with various peak LSPR values. **B)**, **C)**, and **D)** are the TEM images of Ag_2O–Au nanocages with peak LSPR values at 655 nm, 685 nm, and 715 nm, respectively. As the peak LSPR redshifts from 655 nm to 715 nm, the pore size at the wall and corner of the nanocages increases. **E)** HR-TEM image of Ag_2O–Au with the peak LSPR value at 685 nm, the inset shows the Fast Fourier Transform (FFT) of the nanoparticle, confirming the formation of Ag_2O after oxygen treatment. **F)** Lattice spacing of Ag_2O (2.23 Å) and Au (2.68 Å) in the Ag_2O–Au-685 nanoparticle obtained from HRTEM.

oxidation potential is more positive (1.68 V vs. RHE) than the E_{VBM} of photocatalysts. The flat band potential (E_{fb}) of Ag_2O was determined to be 1.31 V vs. RHE, which is close to the E_{VBM} of Ag_2O (1.57 V vs. RHE) [33]. The negative slope of the Mott–Schottky curve confirms that Ag_2O is a p-type semiconductor whose Fermi level energy is lower than that of Au plasmonic metal, indicating the downward bending of the Ag_2O conduction band when it is in contact with Au. Here Au not only provides active catalytic centers for water oxidation and nitrogen reduction through generating hot holes and electrons upon LSPR excitation, but it also collects photo-generated electrons from the Ag_2O semiconductor, retards electron-hole recombination and enhances charge transfer efficiency for NRR.

The photochemical nitrogen fixation tests are carried out in a single-compartment cell using photoelectrodes comprised of indium tin oxide (ITO) supported nanoparticles immersed in N_2-saturated DI water with magnetic stirring under constant N_2 bubbling. The external light source shines through a one-inch quartz window placed in the front side of the cell (Fig. 3B). A 300 W Xe light source provides the air mass (AM) 1.5-irradiance of 100 mW cm-2. The illumination intensity near the sample surface is calibrated using a standard Si-solar cell, and the distance is adjusted to 6 cm to achieve one sun illumination. The cell is placed in the water bath to maintain the reaction temperature constant during the experiment to 20 °C and reduce thermal effects on the photocatalytic rate. The ammonia yield is measured by using the indophenol blue method (Fig. S5).

Among all photoelectrodes tested (i.e., Ag_2O–Au, Ag–Au, Ag_2O, Au), Ag_2O–Au-685 nanocages showed the highest activity, with the ammonia yield of 61.3 mg m^{-2} and η_{STA} of 0.017% after 2 h illumination (Fig. 3C). This high activity is attributed to the combined effects of generated hot electrons by Au nanoparticles and photo-generated electrons by Ag_2O semiconductor that enhanced the photocatalytic NRR. The photocatalytic NH_3 production is further investigated by using a cutoff filter to provide visible light irradiation (400 nm $< \lambda <$ 800 nm). The NH_3 production rate of 47.8 mg m^{-2} is obtained after 2 h visible light illumination with the visible light intensity of 455.2 W m^{-2}, resulting to a $\eta_{STA\text{-}Vis}$ of 0.029% (see supporting information for the detailed calculation, Fig. S6, Table S2). The Ag–Au nanocages (ammonia yield: 36 mg m^{-2}, η_{STA}: 0.01%) exhibit a higher

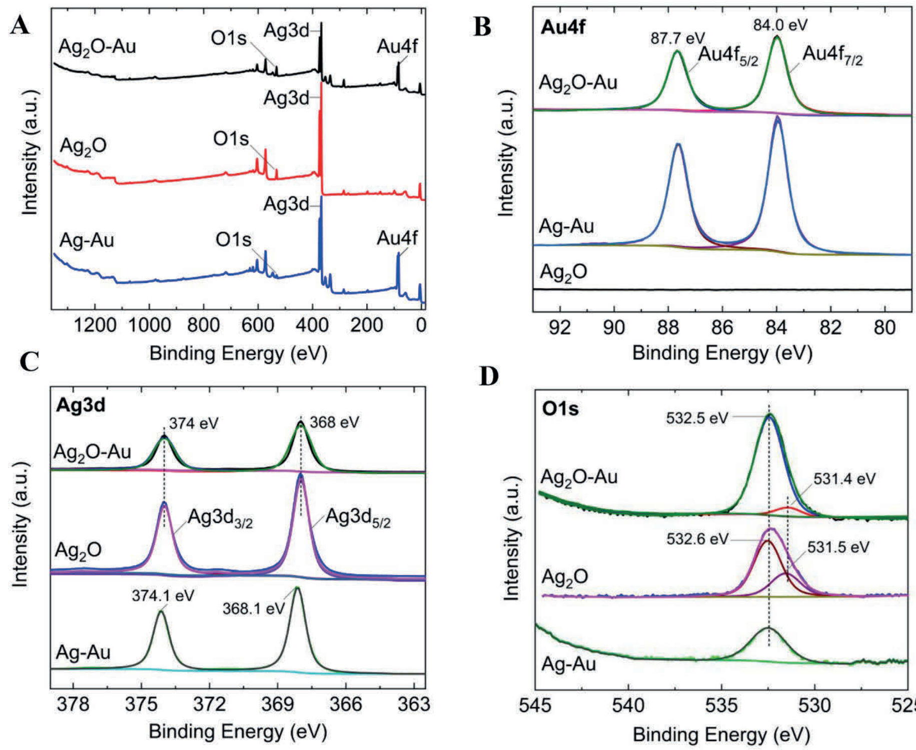

Fig. 2. **A**) XPS survey spectra, **B**) XPS spectra of Au 4f, **C**) Ag 3d, and **D**) O1s for Ag_2O, Ag_2O–Au, and Ag–Au nanoparticles. All spectra were shift corrected using a standard reference C1s, C–C peak at 284.8 eV.

NRR activity than Ag_2O (ammonia yield: 33.5 mg m^{-2}, η_{STA}: 0.0093%). Although it was shown that Ag is not an active site for NRR, Ag–Au nanocages benefit from the "cage effect" and higher active surface area compared with solid Ag_2O nanocubes, which have higher light absorption capability [25]. It is noted that through the oxygen treatment of AgNCs, solid Ag_2O nanocubes are obtained [33]. It should be noted that among all solid Au plasmonic nanoparticles (i.e., nanorods (AuNRs), nanocubes (AuNCs), and nanospheres (AuNSs), Fig. S7), AuNRs reveal the highest NRR activity (ammonia yield: 33.5 mg m^{-2}, η_{STA}: 0.0089%). This is attributed to the two plasmon peaks (transverse (510 nm) and longitudinal (746 nm) modes) observed for AuNRs which brings advantage in light absorption compared with one plasmon peak of AuNCs or AuNSs when all other operating conditions are the same (Fig. 3C, Fig. S7). Even though the current study does not utilize AuNRs, remarkably higher NRR activity is achieved through hybrid nanocages oppose to pure Au nanoparticles. Ag_2O–Au-685 nanocages are further tested throughout 24 h illumination. The ammonia yield rate of 28.2 mg m^{-2} h^{-1} is obtained with N_2 under illumination (N_2, light) (Fig. 3D). Significantly lower ammonia yield rates are achieved in Ar-saturated water with illumination (0.98 mg m^{-2} h^{-1}) and N_2-saturated water without illumination (0.83 mg m^{-2} h^{-1}), indicating that N_2 is the only source of NH_3 obtained by photocatalytic NRR (Fig. 3D). The small amounts of ammonia measured in control experiments could be attributed to the interaction of the adsorbed N_2 at the catalyst surface with water and the leakage of N_2 from the atmosphere into the cell [10,42]. Ag–Au nanocages with various peak LSPR values (i.e., 645, 670, and 710 nm) and pore sizes are tested for photocatalytic NRR for 2 h illumination before (Ag–Au) and after O_2 treatment (Ag_2O–Au) (Fig. 3E). For all nanocages, the ammonia yield increases after O_2 treatment of Ag–Au nanocages, suggesting that the formation of Ag_2O enhances photocatalytic NRR for NH_3 production. In addition, among Ag–Au nanocages with various peak LSPR values before O_2 treatment, the ammonia yield increases as LSPR redshifts from 645 nm to 710 nm. This is attributed to the fact that as LSPR redshifts, Ag is replaced with Au through galvanic replacement, and the Ag content of the nanoparticles decreases (Table S1). This is favorable for increasing photocatalytic activity, as Au is an active nanocatalyst for NRR. Ag_2O–Au-685 nanocages showed the highest photocatalytic NRR activity. This is ascribed to the compromise between the pore size, the active surface area of the nanoparticle, and the Ag content (transformed to Ag_2O after O_2 treatment) of Ag_2O–Au nanocages. Here, higher Ag content (Ag_2O–Au-655 has the highest Ag content, See Table S1) is beneficial, as it is transformed to Ag_2O after O_2 treatment, which provides photo-excited electrons for NRR. In addition, in order to enhance photocatalytic NRR, it is necessary to engineer the optimum pore size; this can be done by tuning the LSPR peak position to obtain the highest active surface area while reactants and products can diffuse in and out of the cavity without restrictions. Here, an optimum Ag content and a pore size that maximizes photocatalytic NRR for NH_3 production are achieved by using Ag_2O–Au-685 nanocages (Fig. 3E). The apparent quantum efficiency (η_{AQE}) is calculated to be 1.2% for Ag_2O–Au-685 nanocages using 685 nm bandpass filter with 15 nm bandwidth at full-width half-maximum (FWHM) which is greater than the highest values currently reported in the literature (Table S3). The light intensity is measured by a standard Si-solar cell, and the NH_3 yield is measured after 2 h of monochromatic light irradiation at 685 nm (See supporting information for detailed calculations of η_{STA} and η_{AQE}). The stability of Ag_2O–Au-685 for photocatalytic NH_3 production is evaluated for 40 h by conducting five consecutive cycles, each for 8 h (assuming 8 h of daylight per day), (Fig. 3F). The photocatalyst could maintain continuous NH_3 formation with a stable NH_3 yield and η_{STA} (92.5% performance retention). In addition, the TEM images and XPS spectra of the photocatalyst before and after the durability test show that the morphology and chemical states of nanoparticles are reasonably maintained after a 40 h photochemical test (Figs. S8 and S9).

The transient photocurrent responses are measured, for ITO supported Ag_2O–Au nanocages with various LSPR peak values, in N_2-saturated 0.5 M $LiClO_4$ aqueous solution to evaluate the interfacial charge kinetics (Fig. 4A). The schematic of the photoelectrochemical setup is provided in the supporting information (Fig. S10). Ag_2O–Au-685

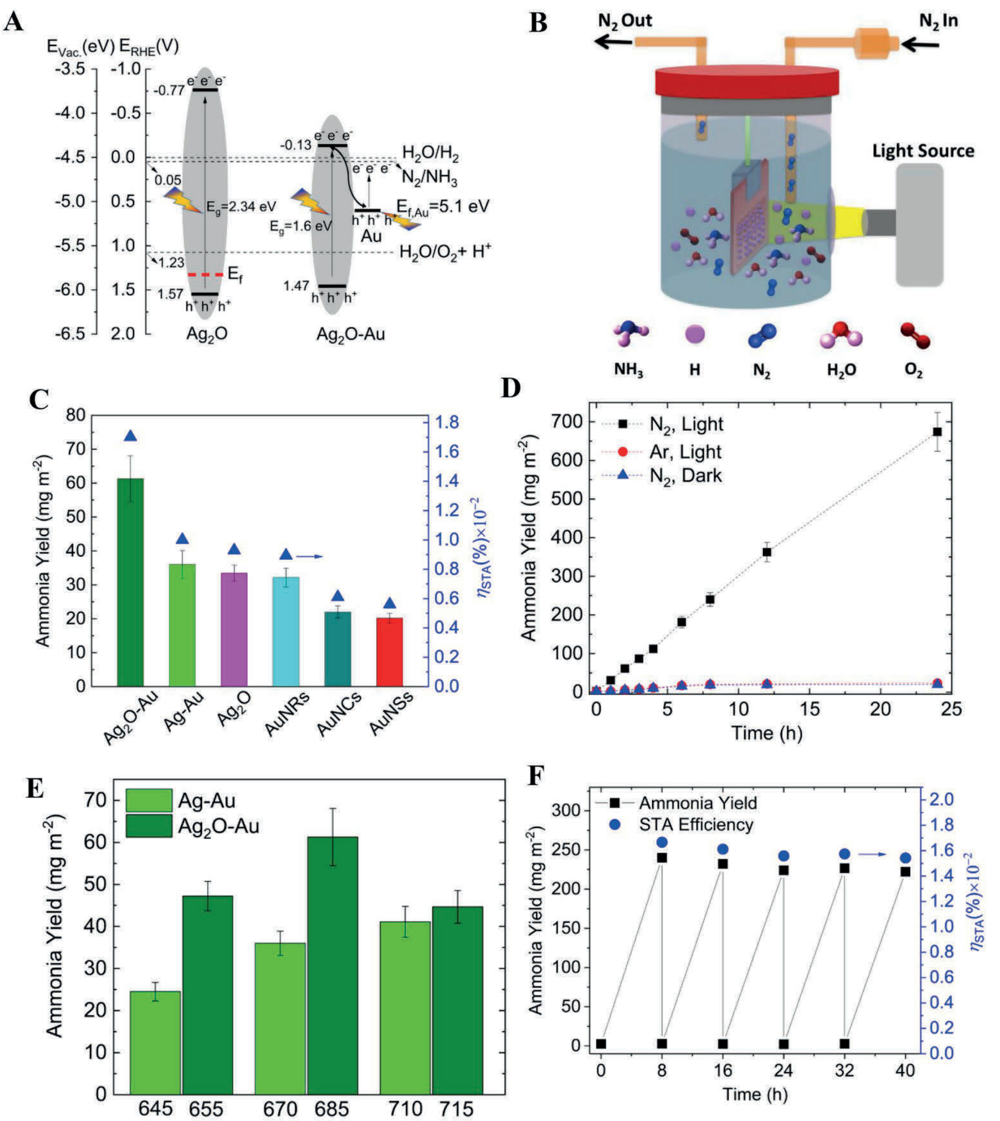

Fig. 3. A) Electronic band structure of Ag_2O and Ag_2O–Au photocatalyst for nitrogen reduction reaction **B)** Schematic of photochemical cell for NRR. **C)** Ammonia yield and solar-to-ammonia (STA) efficiency of various photocatalysts under one sun illumination for 2 h in a N_2 saturated pure water. **D)** Ammonia yield of Ag_2O–Au-685 under various operating conditions over 24 h. **E)** Ammonia yield for photocatalysts with various peak LSPR values before (Ag–Au) and after (Ag2O–Au) oxygen treatment. **F)** Stability test of Ag_2O–Au-685 photoelectrode for ammonia production. Five consecutive tests are carried out for the period of 8 h (total 40 h) using Ag_2O–Au-685 photoelectrode. The electrolyte solution was replaced before starting each cycle.

exhibits the highest photocurrent response, suggesting the efficient charge separation and transfer process using this photocatalyst. This result is in line with the greater photocatalytic activity of NRR for NH_3 production using Ag_2O–Au-685 nanocages. Furthermore, the photocurrent responses are compared in Ar- and N_2-saturated electrolyte using an Ag_2O–Au-685 photoelectrode (Fig. 4B). The higher photocurrent response in Ar-saturated electrolyte (64.3 nA cm^{-2}), compared with N_2-saturated electrolyte (54.1 nA cm^{-2}), is attributed to the two possible pathways for photo-induced electrons in an N_2 atmosphere, where they can either be transferred to the ITO surface (photocurrent response) or to the adsorbed N_2 molecules at the electrode-electrolyte interface. This decreases the number of electrons transferred to the ITO and therefore lowers the photocurrent response in an N_2 atmosphere compared with an Ar atmosphere (Fig. 4B) [40,43]. The values of the transient photocurrent responses of all nanoparticles are provided in the supporting information (Table S1). It is important to note that ammonia yield does not change dramatically under visible light illumination (47.8 mg m^{-2}) and on-plasmon resonance excitation at 685 nm (39.11 mg m^{-2}) (Table S2). The difference between these two values (8.69 mg m^{-2}) is the sole contribution of the Ag_2O semiconductor, which is excited by off-plasmon resonance but has sufficient photon energy to stimulate the Ag_2O. This strongly signifies the plasmonic excitation effect, which is further promoted by charge separation at the plasmonic metal-semiconductor interface. Photoluminescence (PL) measurements are performed to examine the charge transfer for Ag_2O and Ag_2O–Au-685 photocatalysts, and emissions are measured using 375 nm excitation wavelength (Fig. 4C). The emission intensity in the PL spectrum of Ag_2O–Au is remarkably lower than that of Ag_2O, which is attributed to the fluorescence quenching by the Au nanoparticles. Furthermore, Nyquist plots are obtained by performing electrochemical impedance spectroscopy (EIS) under illumination (Fig. 4D). The charge transfer resistance (R_{CT}) of Ag_2O–Au (1.34 kΩ cm^2) is smaller than that of Ag_2O (1.68 kΩ cm^2), suggesting an enhanced transfer of photo-generated charge carriers, which could promote an efficient photocatalytic NRR.

Isotopic labeling experiments using $^{15}N_2$ gas are performed to further confirm the source of NH_3 formation in photochemical NRR tests. The amounts of ammonia produced with $^{14}N_2$ and $^{15}N_2$ after photoirradiation for 4 h is 16.5 μM and 17.1 μM which were analyzed using the indophenol method. The amount of ammonia is further measured by the NMR method. Calibration curves of the ^1H NMR signal for standard solutions of $^{15}NH_4{}^+$ and $^{14}NH_4{}^+$ are provided in the supporting information (Fig. S11). ^1H NMR spectrum obtained from the sample in the photochemical $^{14}N_2$ reduction experiment lie at a chemical shift of triplet coupling of $^{14}N_2$ similar to that of standard $^{14}NH_4{}^+$ samples (J-coupling: 52 Hz). Doublet coupling of $^{15}N_2$ (J-coupling: 73 Hz) is obtained after photochemical $^{15}N_2$ reduction reaction which agrees well with the standard $^{15}NH_4{}^+$ solution. A small amount of

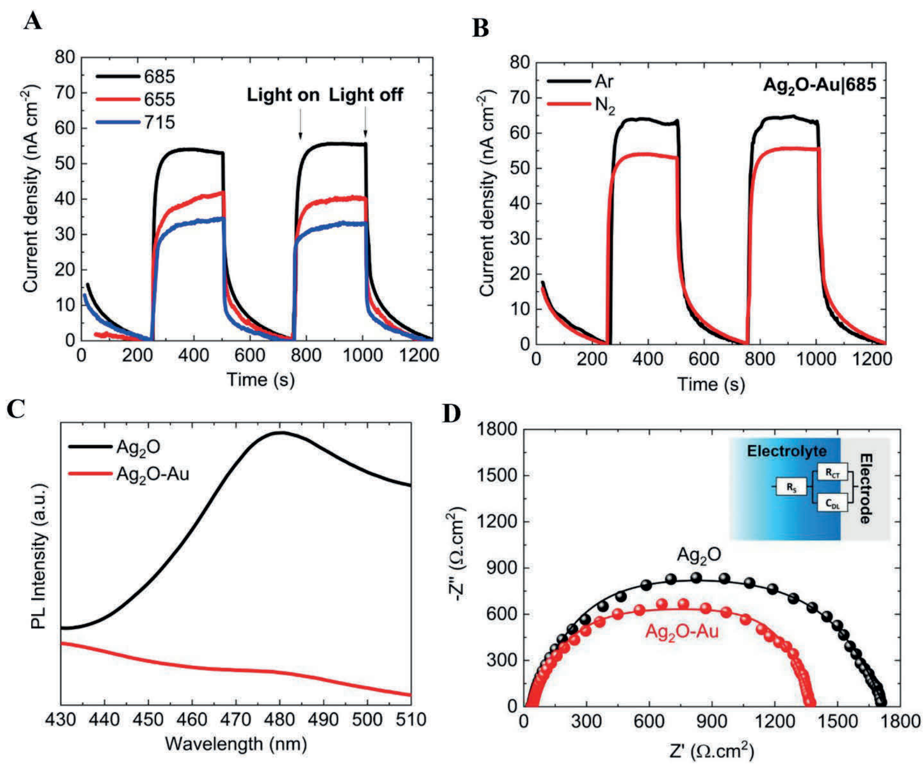

Fig. 4. A) Transient photocurrent response of Ag_2O–Au with various LSPR peak values, **B**) Transient photocurrent response of Ag_2O–Au-685 in N_2 and Ar saturated 0.5 M $LiClO_4$ aqueous solution under 1 sun illumination. Photocurent responses are measured at the open circuit voltage of the cell **C**) Photoluminescence spectra of Ag_2O and Ag_2O–Au-685 photocatalysts. Both samples were excited with 375 nm excitation source. **D**) Nyquist plots of the Ag_2O–Au-685 under photoirradiation at an applied potential of 0.5 V (vs Ag/AgCl) in 0.5 M $LiClO_4$ aqueous solution. The equivalent circuit model in the inset comprises charge transfer resistance (R_{CT}), double layer capacitance (C_{DL}), and ohmic resistance (R_S). R_{CT} was obtained from the diameter of semicircles for each photocatalyst.

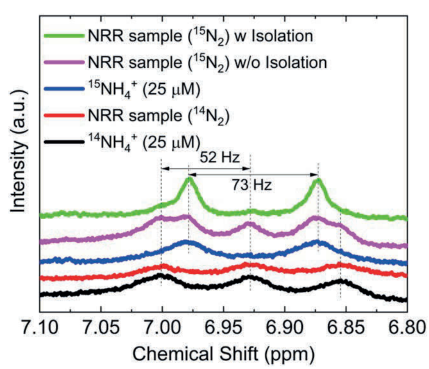

Fig. 5. ^{1}H-NMR spectra of samples after photochemical $^{15}N_2$ ($^{14}N_2$) reduction reaction under 1-sun illumination for 4 h using Ag_2O–Au-685 nanocages and standard $^{15}NH_4^+$ and $^{14}NH_4^+$ samples.

$^{14}NH_4^+$ is observed (~ 4 μM) after $^{15}N_2$ reduction experiments, indicating the possible leakage of $^{14}N_2$ from the atmosphere into the cell (Fig. 5). By carefully isolating the cell and maintaining a slight positive pressure of $^{15}N_2$ through connecting the cell's headspace to the gas sampling bag, we successfully decreased the leakage of $^{14}N_2$ (Fig. 5) [42]. The amount of ammonia quantified using ^{1}H NMR measurement is very close to the amount of ammonia measured using indophenol method (16.9 μM for $^{14}NH_4^+$ and 16.6 μM for $^{15}NH_4^+$ using ^{1}H NMR measurements) which further confirms that the supplied N_2 gas is the major source of NH_3 formation in our system.

3. Conclusion

Photo(electro)catalytic nitrogen fixation was demonstrated in a pure water system without using sacrificial reagents, under atmospheric pressure and room temperature, and using a visible-light-responsive hybrid hollow plasmonic-semiconductor photocatalyst. At a peak LSPR of 685 nm, a η_{STA} of 0.017% and a η_{AQE} of 1.2% after 2 h monochromatic light irradiation at 685 nm was achieved. The Ag content and pore size were shown to be the key elements for optimizing the photocatalytic activity of NRR using Ag_2O–Au nanocages with various LSPR peak positions. Furthermore, the enhanced activity of Ag_2O–Au compared with Ag–Au is attributed to the contribution of photo-generated electrons after photo-excitation, owing to the formation of Ag_2O after O_2 treatment of Ag–Au nanocages, which were revealed by photochemical testing.

This work opens up a new avenue for the design of an efficient visible-light responsive hybrid hollow plasmonic-semiconductor photoelectrode with broad applications in the photo(electro)chemical energy conversion systems.

4. Experimental section

Photochemical Nitrogen Reduction: The photocatalytic NRR measurements were carried out in a single-compartment cell using various photoelectrodes comprised of indium tin oxide (ITO) supported nanoparticles immersed in N_2-saturated DI water with magnetic stirring under constant N_2 bubbling at the flow rate of 20 mL min^{-1}. Nitrogen (Ar gas for control experiments) gas was bubbled through the cell for 1 h before starting the photochemical measurements to remove dissolved oxygen gas. To prepare the photoelectrode for the photo(electro) chemical tests, 300 μL of nanoparticles of known concentrations (Table S1) and 1.5 μL of Nafion solution (5% wt.) were sonicated and drop casted onto a square of indium tin oxide (ITO) (1cm×1cm) and then dried under N_2 atmosphere at 75 °C for 1 h. The photoelectrode was then attached to Ni wire with conductive silver paint and isolated from the electrolyte using epoxy. The air mass (AM) 1.5-irradiance of 100 mW cm^{-2} was provided by a 300 W Xe light source. The illumination intensity near the sample surface was calibrated using a standard Si-solar cell and the distance was adjusted to 6 cm to achieve 1 sun illumination. The cell was placed in the water bath to maintain the reaction temperature constant during the experiment to 20 °C and reduce thermal effects on the photocatalytic rate.

The solar-to-ammonia efficiency (η_{STA}) is calculated according to the following equation:

$$\eta_{STA}\ (\%) = \frac{\Delta G\ for\ ammonia\ generation\ (J\ mol^{-1}) \times ammonia\ generated\ (mol)}{input\ light\ energy\ (J\ s^{-1}) \times reaction\ time\ (s)} \times 100 \quad (4)$$

The free energy for NH_3 generation is 339 kJ mol^{-1} and the input light energy is 1000 J s^{-1}.

The apparent quantum efficiency (QE) of the NH_3 production using 685 nm bandpass filter with 15 nm FWHM is calculated as follows:

$$QE\ (\%) = \frac{NH_3\ generated\ (mol) \times 3}{the\ number\ of\ incident\ photons\ \ (mol)} \times 100 \quad (5)$$

The light intensity is measured to be 14 W m^{-2}, and NH_3 yield is measured after 2 h monochromatic light irradiation at 685 nm.

Acknowledgments

This material is based upon work supported by the National Science Foundation under Grant No. 1904351. Materials characterization was performed at the Georgia Tech Institute for Electronics and Nanotechnology (IEN), a member of the National Nanotechnology Coordinated Infrastructure, which is supported by the National Science Foundation (Grant ECCS-1542174). The authors thank Dr. S. R. Panikkanvalappil for performing PL measurements of nanoparticles. The authors are also grateful to Luke Soule and Prof. Meilin Liu for helpful discussions.

Appendix A. Supplementary data

Supplementary data to this article can be found online at https://doi.org/10.1016/j.nanoen.2019.103886.

References

[1] V. Smil, Nitrogen cycle and world food production, World Agric. 2 (1) (2011) 9–13.
[2] D.E. Canfield, A.N. Glazer, P.G. Falkowski, The evolution and future of Earth's nitrogen cycle, Science 330 (6001) (2010) 192–196.
[3] R. Lan, S. Tao, Ammonia as a suitable fuel for fuel cells, Front. Energy Res. 2 (2014) 35.
[4] J.-L. Ma, D. Bao, M.-M. Shi, J.-M. Yan, X.-B. Zhang, Reversible nitrogen fixation based on a rechargeable lithium-nitrogen battery for energy storage, Chem 2 (4) (2017) 525–532.
[5] D. Bao, Q. Zhang, F.L. Meng, H.X. Zhong, M.M. Shi, Y. Zhang, J.M. Yan, Q. Jiang, X.B. Zhang, Electrochemical reduction of N2 under ambient conditions for artificial N2 fixation and renewable energy storage using N2/NH3 cycle, Adv. Mater. 29 (3) (2017) 1604799.
[6] P. Arora, I. Sharma, A. Hoadley, S. Mahajani, A. Ganesh, Remote, small-scale, 'greener' routes of ammonia production, J. Clean. Prod. 199 (2018) 177–192 10/20/2018.
[7] S. Linic, P. Christopher, D.B. Ingram, Plasmonic-metal nanostructures for efficient conversion of solar to chemical energy, Nat. Mater. 10 (12) (2011) 911.
[8] G. Schrauzer, T. Guth, Photocatalytic reactions. 1. Photolysis of water and photoreduction of nitrogen on titanium dioxide, J. Am. Chem. Soc. 99 (22) (1977) 7189–7193.
[9] G.N. Schrauzer, Photoreduction of nitrogen on TiO_2 and TiO_2-containing minerals, Energy Efficiency and Renewable Energy through Nanotechnology, Springer, 2011, pp. 601–623.
[10] H. Hirakawa, M. Hashimoto, Y. Shiraishi, T. Hirai, Photocatalytic conversion of nitrogen to ammonia with water on surface oxygen vacancies of titanium dioxide, J. Am. Chem. Soc. 139 (31) (2017) 10929–10936.
[11] O. Rusina, A. Eremenko, G. Frank, H.P. Strunk, H. Kisch, Nitrogen photofixation at nanostructured iron titanate films, Angew. Chem. Int. Ed. 40 (21) (2001) 3993–3995.
[12] O. Rusina, O. Linnik, A. Eremenko, H. Kisch, Nitrogen photofixation on nanostructured iron titanate films, Chem. Eur J. 9 (2) (2003) 561–565.
[13] X. Chen, N. Li, Z. Kong, W.-J. Ong, X. Zhao, Photocatalytic fixation of nitrogen to ammonia: state-of-the-art advancements and future prospects, Mater. Horiz. 5 (1) (2018) 9–27.
[14] H. Li, J. Shang, Z. Ai, L. Zhang, Efficient visible light nitrogen fixation with BiOBr nanosheets of oxygen vacancies on the exposed {001} facets, J. Am. Chem. Soc. 137 (19) (2015) 6393–6399.
[15] J. Li, H. Li, G. Zhan, L. Zhang, Solar water splitting and nitrogen fixation with layered bismuth oxyhalides, Accounts Chem. Res. 50 (1) (2016) 112–121.
[16] X. Xue, R. Chen, H. Chen, Y. Hu, Q. Ding, Z. Liu, L. Ma, G. Zhu, W. Zhang, Q. Yu, J. Liu, Oxygen vacancy engineering promoted photocatalytic ammonia synthesis on ultrathin two-dimensional bismuth oxybromide nanosheets, Nano Lett. 18 (11) (2018) 7372–7377.
[17] S.V. Boriskina, H. Ghasemi, G. Chen, Plasmonic materials for energy: from physics to applications, Mater. Today 16 (10) (2013) 375–386.
[18] K. Saha, S.S. Agasti, C. Kim, X. Li, V.M. Rotello, Gold nanoparticles in chemical and biological sensing, Chem. Rev. 112 (5) (2012) 2739–2779.
[19] W.A. Murray, W.L. Barnes, Plasmonic materials, Adv. Mater. 19 (22) (2007) 3771–3782.
[20] M.A. Mahmoud, D. O'Neil, M.A. El-Sayed, Hollow and solid metallic nanoparticles in sensing and in nanocatalysis, Chem. Mater. 26 (1) (2013) 44–58.
[21] C. Clavero, Plasmon-induced hot-electron generation at nanoparticle/metal-oxide interfaces for photovoltaic and photocatalytic devices, Nat. Photon. 8 (2) (2014) 95.
[22] M. Ali, F. Zhou, K. Chen, C. Kotzur, C. Xiao, L. Bourgeois, X. Zhang, D.R. MacFarlane, Nanostructured photoelectrochemical solar cell for nitrogen reduction using plasmon-enhanced black silicon, Nat. Commun. 7 (2016) 11335.
[23] C. Hu, X. Chen, J. Jin, Y. Han, S. Chen, H. Ju, J. Cai, Y. Qiu, C. Gao, C. Wang, Z. Qi, Surface plasmon enabling nitrogen fixation in pure water through a dissociative mechanism under mild conditions, J. Am. Chem. Soc. 141 (19) (2019) 7807–7814.
[24] M.K. Gupta, T. König, R. Near, D. Nepal, L.F. Drummy, S. Biswas, S. Naik, R.A. Vaia, M.A. El-Sayed, V.V. Tsukruk, Surface assembly and plasmonic properties in strongly coupled segmented gold nanorods, Small 9 (17) (2013) 2979–2990.
[25] M. Nazemi, M.A. El-Sayed, Electrochemical synthesis of ammonia from N_2 and H_2O under ambient conditions using pore-size-controlled hollow gold nanocatalysts with tunable plasmonic properties, J. Phys. Chem. Lett. 9 (17) (2018) 5160–5166.
[26] M. Nazemi, S.R. Panikkanvalappil, M.A. El-Sayed, Enhancing the rate of electrochemical nitrogen reduction reaction for ammonia synthesis under ambient conditions using hollow gold nanocages, Nano Energy 49 (2018) 316–323.
[27] T. Oshikiri, K. Ueno, H. Misawa, Plasmon-induced ammonia synthesis through nitrogen photofixation with visible light irradiation, Angew. Chem. Int. Ed. 53 (37) (2014) 9802–9805.
[28] T. Oshikiri, K. Ueno, H. Misawa, Selective dinitrogen conversion to ammonia using water and visible light through plasmon-induced charge separation, Angew. Chem. 128 (12) (2016) 4010–4014.
[29] C. Li, T. Wang, Z.J. Zhao, W. Yang, J.F. Li, A. Li, Z. Yang, G.A. Ozin, J. Gong, Promoted fixation of molecular nitrogen with surface oxygen vacancies on plasmon-enhanced TiO2 photoelectrodes, Angew. Chem. Int. Ed. 57 (19) (2018) 5278–5282.
[30] J. Yang, Y. Guo, R. Jiang, F. Qin, H. Zhang, W. Lu, J. Wang, J.C. Yu, High-efficiency "Working-in-Tandem" nitrogen photofixation achieved by assembling plasmonic gold nanocrystals on ultrathin titania nanosheets, J. Am. Chem. Soc. 140 (27) (2018) 8497–8508.
[31] E. Shi, Y. Gao, B.P. Finkenauer, A.H. Coffey, L. Dou, Two-dimensional halide perovskite nanomaterials and heterostructures, Chem. Soc. Rev. 47 (16) (2018) 6046–6072.
[32] H. Cheng, B. Huang, Y. Dai, Engineering BiOX (X= Cl, Br, I) nanostructures for highly efficient photocatalytic applications, Nanoscale 6 (4) (2014) 2009–2026.
[33] M. Nazemi, M.A. El-Sayed, The role of oxidation of silver in bimetallic gold–silver nanocages on electrocatalytic activity of nitrogen reduction reaction, J. Phys. Chem. C 123 (18) (2019) 11422–11427.
[34] A. Kafizas, S.A. Parry, A.V. Chadwick, C.J. Carmalt, I.P. Parkin, An EXAFS study on the photo-assisted growth of silver nanoparticles on titanium dioxide thin-films and the identification of their photochromic states, Phys. Chem. Chem. Phys. 15 (21) (2013) 8254–8263.
[35] D.B. Akolekar, S.K. Bhargava, G. Foran, EXAFS studies on gold nanoparticles over novel catalytic materials, Radiat. Phys. Chem. 75 (11) (2006) 1948–1952.
[36] M.M. Shi, D. Bao, B.R. Wulan, Y.H. Li, Y.F. Zhang, J.M. Yan, Q. Jiang, Au sub--nanoclusters on TiO2 toward highly efficient and selective electrocatalyst for N2 conversion to NH3 at ambient conditions, Adv. Mater. 29 (17) (2017) 1606550.
[37] L. Shi, L. Liang, J. Ma, F. Wang, J. Sun, Enhanced photocatalytic activity over the Ag2O–gC 3N4 composite under visible light, Catal. Sci. Technol. 4 (3) (2014) 758–765.
[38] M. Xu, L. Han, S. Dong, Facile fabrication of highly efficient g-C3N4/Ag2O heterostructured photocatalysts with enhanced visible-light photocatalytic activity, ACS Appl. Mater. Interfaces 5 (23) (2013) 12533–12540.
[39] Y. Chao, P. Zhou, N. Li, J. Lai, Y. Yang, Y. Zhang, Y. Tang, W. Yang, Y. Du, D. Su, Y. Tan, Ultrathin visible-light-driven Mo incorporating In2O3–ZnIn2Se4 Z-scheme nanosheet photocatalysts, Adv. Mater. 31 (5) (2019) 1807226.
[40] C. Xu, P. Qiu, L. Li, H. Chen, F. Jiang, X. Wang, Bismuth subcarbonate with designer defects for broad-spectrum photocatalytic nitrogen fixation, ACS Appl. Mater. Interfaces 10 (30) (2018) 25321–25328.
[41] D.P. Kumar, E.H. Kim, H. Park, S.Y. Chun, M. Gopannagari, P. Bhavani, D.A. Reddy, J.K. Song, T.K. Kim, Tuning band Alignments and charge-transport properties through MoSe2 bridging between MoS2 and cadmium sulfide for enhanced hydrogen production, ACS Appl. Mater. Interfaces 10 (31) (2018) 26153–26161.
[42] X. Yang, J. Nash, J. Anibal, M. Dunwell, S. Kattel, E. Stavitski, K. Attenkofer, J.G. Chen, Y. Yan, B. Xu, Mechanistic insights into electrochemical nitrogen reduction reaction on vanadium nitride nanoparticles, J. Am. Chem. Soc. 140 (41) (2018) 13387–13391.
[43] N. Zhang, A. Jalil, D. Wu, S. Chen, Y. Liu, C. Gao, W. Ye, Z. Qi, H. Ju, C. Wang, X. Wu, Refining defect states in W18O49 by Mo doping: a strategy for tuning N2 activation towards solar-driven nitrogen fixation, J. Am. Chem. Soc. 140 (30) (2018) 9434–9443.

2**Mohammadreza Nazemi** is a Ph.D. candidate at the Laser Dynamics Laboratory under the supervision of Prof. Mostafa A. El-Sayed at the Georgia Institute of Technology. He received his BS degree (2013) in Aerospace Engineering from the Sharif University of Technology and MS degree (2015) in Mechanical Engineering from Michigan Technological University. His current research focuses on the development and testing of hollow plasmonic nanostructures for photoelectrochemical energy generation. In addition, he is using ultrafast spectroscopy to study the energy transfer in plasmonic nanomaterials and semiconductors.

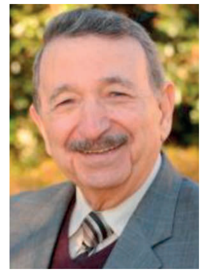

3**Mostafa A. El-Sayed** is the director of the Laser Dynamics Laboratory, Regents' Professor and Julius Brown Chair in the School of Chemistry and Biochemistry at Georgia Tech. He obtained his Ph.D. from Florida State University in 1959 with Michael Kasha, and after postdoctoral fellowships at Harvard, Yale, and Caltech, he joined the faculty of School of Chemistry and Biochemistry at UCLA in 1961 and Georgia Tech later in 1994. He is currently an elected member of the U.S. National Academy of Science, an elected fellow of the American Academy of Arts and Sciences, former editor-in-chief of the Journal of Physical Chemistry. He is the recipient of several prestigious awards including ACS Priestly medal, Ahmed Zewail prize in molecular sciences, the ACS Irving Langmuir Prize in Chemical Physics, the Glenn T. Seaborg Medal, and the U.S. National Medal of Science.